

Noise-Aware and Dynamically Adaptive Federated Defense Framework for SAR Image Target Recognition

Yuchao Hou, *Member, IEEE*, Zixuan Zhang, Jie Wang, Wenke Huang, Lianhui Liang, *Senior Member, IEEE*, Di Wu, *Senior Member, IEEE*, Zhiqian Liu, *Senior Member, IEEE*, Youliang Tian, *Senior Member, IEEE*, Jianming Zhu, Jisheng Dang, Junhao Dong, and Zhongliang Guo

Abstract—As a critical application of computational intelligence in remote sensing, deep learning-based synthetic aperture radar (SAR) image target recognition facilitates intelligent perception but typically relies on centralized training, where multi-source SAR data are uploaded to a single server, raising privacy and security concerns. Federated learning (FL) provides an emerging computational intelligence paradigm for SAR image target recognition, enabling cross-site collaboration while preserving local data privacy. However, FL confronts critical security risks, where malicious clients can exploit SAR’s multiplicative speckle noise to conceal backdoor triggers, severely challenging the robustness of the computational intelligence model. To address this challenge, we propose NADAFD, a noise-aware and dynamically adaptive federated defense framework that integrates frequency-domain, spatial-domain, and client-behavior analyses to counter SAR-specific backdoor threats. Specifically, we introduce a frequency-domain collaborative inversion mechanism to expose cross-client spectral inconsistencies indicative of hidden backdoor triggers. We further design a noise-aware adversarial training strategy that embeds Gamma-distributed speckle characteristics into mask-guided adversarial sample generation to enhance robustness against both backdoor attacks and SAR speckle noise. In addition, we present a dynamic health assessment module that tracks client update behaviors across

Manuscript received XX XX, 2025; revised XX XX, 202X; accepted XX XX, 202X. Date of publication XX XX, 202X; date of current version XX XX, 202X. This work was supported in part by the National Key Research and Development Program of China under Grant 2021YFB3101100, in part by the National Natural Science Foundation of China under Grant 62272123, 42371470, and 42461057, in part by the Fundamental Research Program of Shanxi Province under Grant 202303021212164. (Corresponding authors: Zhongliang Guo and Junhao Dong.)

Yuchao Hou is with the Shanxi Key Laboratory of Cryptography and Data Security, School of Computer Science and Artificial Intelligence, Shanxi Normal University, Taiyuan 030031, China, and the School of Computer Science and Technology, Guizhou University, Guiyang 550025, China (e-mail: yuchaozhou@126.com).

Zixuan Zhang and Jie Wang are with the Shanxi Key Laboratory of Cryptography and Data Security, School of Computer Science and Artificial Intelligence, Shanxi Normal University, Taiyuan 030031, China.

Wenke Huang and Junhao Dong are with the School of Computer Science and Engineering, Nanyang Technological University, Singapore 639798, Singapore (e-mail: junhao003@ntu.edu.sg).

Lianhui Liang is with the School of Electrical Engineering, Guangxi University, Nanning 530004, China.

Di Wu is with the School of Computing, Engineering and Mathematical Science, La Trobe University, Plenty Road, Bundoora, VIC 3086, Australia.

Zhiqian Liu is with the College of Cyber Security, Jinan University, Guangzhou 510632, China.

Youliang Tian is with the School of Computer Science and Technology, Guizhou University, Guiyang 550025, China.

Jianming Zhu is with the School of Information, Central University of Finance and Economics, Beijing 100081, China.

Jisheng Dang is with the School of Information Science and Engineering, Lanzhou University, Lanzhou 730000, China

Zhongliang Guo is with the School of Computer Science, University of St Andrews, St Andrews, KY16 9AJ, United Kingdom (e-mail: zg34@st-andrews.ac.uk).

training rounds and adaptively adjusts aggregation weights to mitigate evolving malicious contributions. Experiments on MSTAR and OpenSARShip datasets demonstrate that NADAFD achieves higher accuracy on clean test samples and a lower backdoor attack success rate on triggered inputs than existing federated backdoor defenses for SAR target recognition.

Index Terms—Synthetic aperture radar (SAR), federated learning (FL), image target recognition, backdoor attack.

I. INTRODUCTION

SYNTHETIC aperture radar (SAR) [1] serves as a foundational sensor for ambient intelligence and Smart-Earth applications, utilizing its high-resolution imaging and all-weather capabilities to enable continuous environmental monitoring [2]. Within this domain, Automatic Target Recognition (ATR) [3] has evolved beyond simple classification into a complex computational intelligence task, requiring systems to emulate cognitive visual processing to robustly interpret targets under variable conditions. This places SAR ATR at the intersection of intelligent sensing and advanced pattern recognition, aligning with the pursuit of autonomous and robust machine intelligence.

However, realizing such intelligent perception faces significant hurdles due to the inherent complexity of SAR imagery. While deep learning models [4] offer powerful representational capacities superior to early handcrafted features, they typically rely on a centralized training paradigm. This architecture is increasingly ill-suited for modern distributed sensing networks, as it incurs prohibitive communication overheads and intensifies privacy and security vulnerabilities [5] by aggregating sensitive raw data, as illustrated in Fig. 1(a).

Federated learning (FL) has emerged as a decentralized paradigm that mitigates privacy concerns by retaining raw SAR data on local devices while only exchanging model parameters or gradients [6], [7]. This design is particularly suitable for SAR image target recognition [8], as it minimizes data exposure and enhances the protection of sensitive information. However, FL also introduces additional security vulnerabilities [9], especially backdoor attacks, as depicted in Fig. 1(b). In SAR scenarios, adversaries may compromise client devices, such as via sensor spoofing, to inject hidden trigger patterns into local datasets. Consequently, the global model may gradually learn these malicious behaviors [10], exhibiting normal performance on clean inputs while misclassifying samples containing the trigger [11]. Due to the decentralized design of FL, server-side auditing is limited, making it difficult to detect such attacks, which allows them

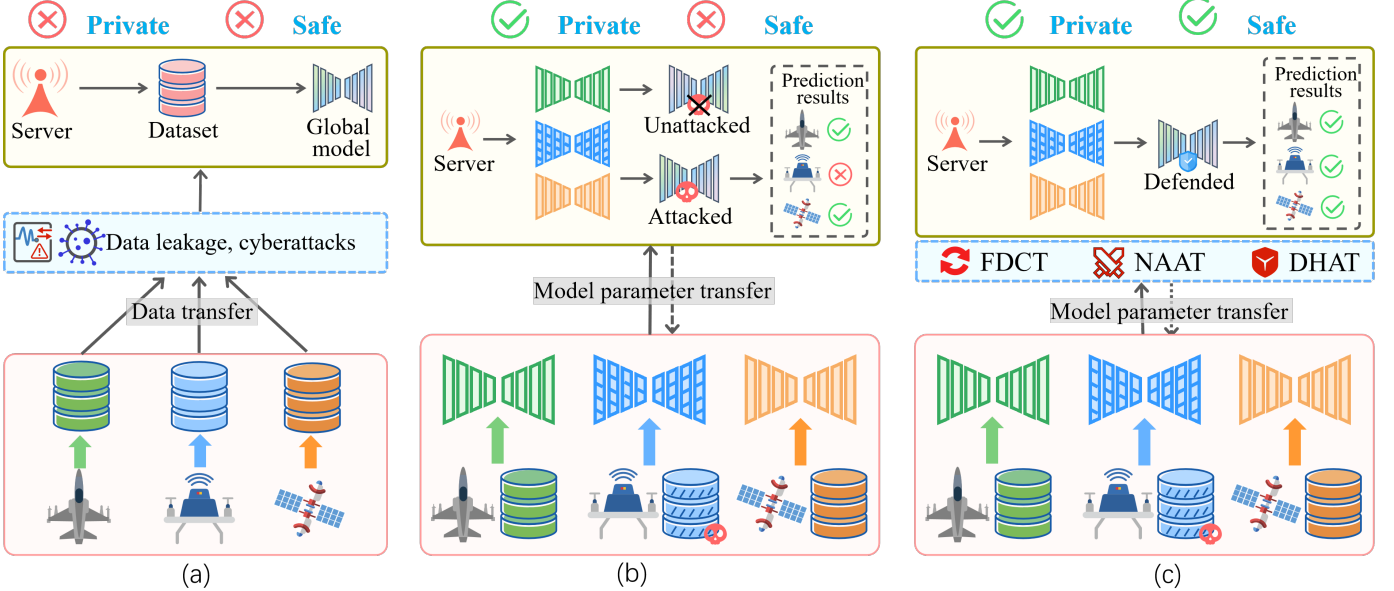


Fig. 1: Comparison of three learning paradigms for SAR target recognition. (a) Centralized learning. (b) Federated learning with security risks. (c) Our proposed defence framework.

to persist across rounds and continuously influence the global model.

Existing defenses against backdoor attacks can be broadly divided into two major categories: behavioral analysis [12] and anomaly detection [13]. The former identifies hidden triggers by examining model prediction behaviors or activation statistics, while the latter flags malicious clients through statistical anomalies in gradients or model updates. However, these paradigms have been predominantly designed and validated on natural images, which typically exhibit relatively smooth textures and stable additive noise characteristics [14]. In stark contrast, SAR images suffer from multiplicative speckle noise that is often modeled by a Gamma distribution [15], which significantly distorts image edges, textures, and frequency-domain representations [16]. This noise-induced spectral interference makes benign spectral variations difficult to distinguish from subtle backdoor trigger patterns. As a result, both behavioral analysis and anomaly-detection defenses exhibit substantially degraded effectiveness when naively applied to SAR-oriented FL systems.

To address these challenges, we propose NADAFD, a noise-aware and dynamically adaptive federated defense framework for SAR target recognition. Our framework establishes a closed-loop defense mechanism that integrates detection, response, and adaptive regulation. In each communication round, clients independently train their models on local SAR datasets and submit updates to a central server. The server then performs frequency-domain analysis across client updates to detect potential backdoor triggers. When anomalies are detected, the server generates adversarial samples based on SAR-specific noise modeling to enhance model robustness. These adversarial examples, along with the original data, are then distributed to the clients for retraining. Subsequently, the server dynamically assesses each client's health based on observed training behavior and adjusts aggregation weights and defense parameters accordingly to suppress evolving malicious

influence. Through this iterative process, NADAFD provides a robust and adaptive defense framework tailored for FL in SAR, as illustrated in Fig. 1(c). Our key contributions are summarized as follows:

- We introduce a federated defense paradigm that incorporates wavelet-domain spectral perception and adaptive behavioral reasoning to localize triggers by analyzing discordance within the distributed collective intelligence.
- We design a training strategy that models SAR speckle noise using Gamma distributions to generate adversarially robust samples with enhanced physical plausibility, and leverage spatial-channel attention to focus on key discriminative regions.
- We further propose a dynamic health assessment mechanism that evaluates client training behavior and adjusts aggregation weights accordingly. This feedback-driven process improves adaptability against evolving attacks while maintaining stable model convergence.

The remainder of this paper is organized as follows. Section II reviews related work. Section III details the proposed NADAFD framework. Section IV presents the experimental setup and results. Finally, Section V concludes the paper.

II. RELATED WORK

A. SAR Image Target Recognition

SAR imagery has become an indispensable data modality for intelligent perception in a wide range of critical applications, including military reconnaissance, terrain mapping, and disaster monitoring [17], [18]. The field of SAR target recognition has evolved from traditional handcrafted-feature methods toward data-driven deep learning. The advent of convolutional neural networks (CNNs) marked a major breakthrough, with models leveraging mechanisms such as multi-scale fusion and attention to substantially improve accuracy under challenging

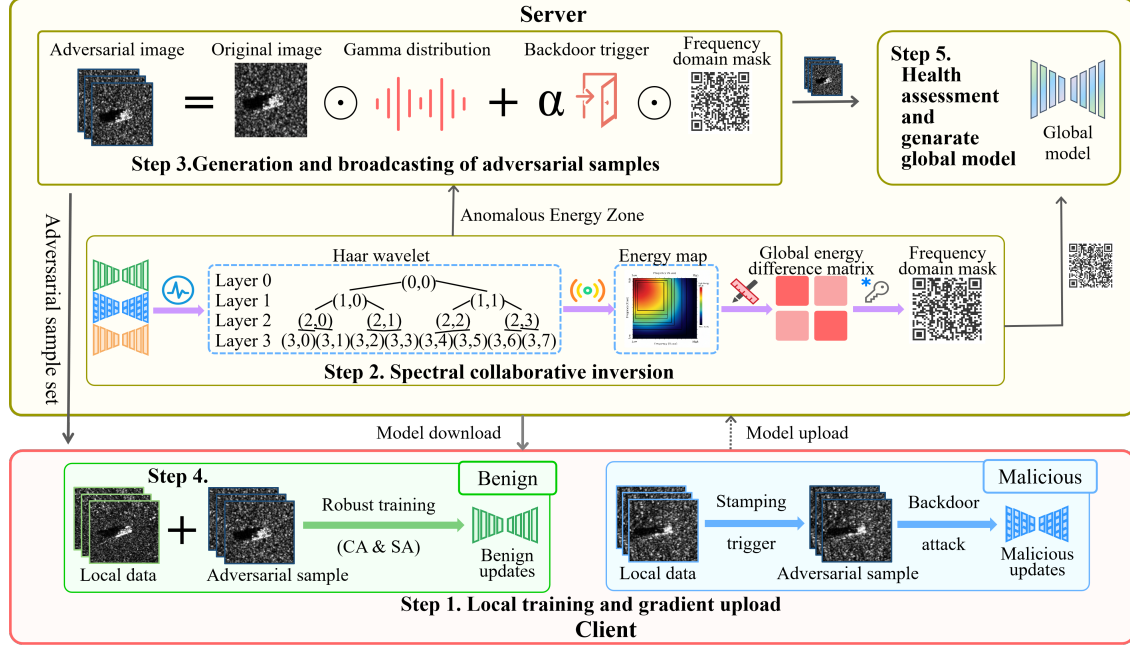


Fig. 2: Pipeline of our proposed framework.

conditions like low signal-to-noise ratio [19], [20]. Furthermore, to address the inherent complexities of SAR data, noise-robust modules and despeckling strategies have been integrated into modern frameworks to enhance robustness [21].

Despite these advancements, the inherent presence of speckle noise remains a fundamental obstacle to reliable SAR target recognition [22]. Originating from the coherent processing of radar echoes, SAR speckle is statistically characterized by a Gamma distribution [15], [23]. Unlike additive noise, it is multiplicative and spatially correlated, rendering its suppression intrinsically challenging: overly aggressive filtering inevitably erodes structural and edge details that are critical for accurate recognition. Such degradation of low-level image features directly weakens the discriminative capacity of recognition models and may further destabilize the training process [24]. Although existing countermeasures span from traditional filtering techniques [25] to modern deep learning-based despeckling approaches [26], the former are often constrained by stationary noise assumptions and struggle to accommodate the non-stationary and heterogeneous characteristics of real SAR speckle.

In summary, while deep learning has driven substantial progress in SAR ATR, two intertwined limitations persist: a reliance on centralized data aggregation that conflicts with practical privacy and deployment constraints, and an insufficient inherent robustness to the statistical and structural distortions induced by SAR speckle noise. These limitations collectively highlight the need for a learning paradigm that is decentralized, privacy-preserving, and explicitly aware of SAR-specific noise characteristics, thereby motivating the adaptation of FL to the SAR ATR domain.

B. Backdoor Vulnerabilities in FL

FL has emerged as a compelling paradigm for SAR target recognition, as its decentralized training protocol naturally aligns with the distributed acquisition and deployment characteristics of SAR systems. By enabling collaborative model optimization without centralizing sensitive data, FL effectively mitigates privacy concerns while reducing communication overhead [27]. Prior studies have further demonstrated that FL can maintain, or even enhance, recognition robustness under practical constraints such as non-identically distributed (non-IID) data distributions and limited local samples [28], underscoring its suitability for large-scale and heterogeneous SAR scenarios.

However, backdoor attacks pose a significant threat to FL, as compromised clients can poison local data or manipulate gradient updates [29] to embed hidden triggers into the global model, leading to misclassification of trigger-bearing inputs while preserving high accuracy on benign samples [30]. This threat is amplified in SAR applications due to speckle noise and complex scattering mechanisms, which inherently obscure and disguise adversarial perturbations. Attackers can craft triggers in spectrally dominant low-frequency bands or design perturbations that mimic heavy-tailed speckle statistics, greatly reducing the effectiveness of standard anomaly detection or gradient-based defenses [31].

Despite extensive efforts to defend against backdoor attacks in federated settings, most existing approaches are developed under assumptions tailored to natural images and therefore fail to generalize to SAR imagery. Detection- and aggregation-based defenses, such as Krum [32] and FSBA [13], rely on identifying statistical outliers among client updates, but frequently misinterpret benign, speckle-induced gradient variability as adversarial behavior, leading to excessive false positives. Similarly, frequency-aware aggregation strategies [33]

typically assume additive or Gaussian noise models, which are fundamentally incompatible with the multiplicative and non-Gaussian nature of SAR speckle. Model purification techniques based on synthetic noise injection or denoising transformations [34] further struggle to preserve the complex spatial correlations and textural structures intrinsic to SAR images, often resulting in incomplete backdoor removal or unnecessary degradation of recognition performance.

These shortcomings highlight the critical need for SAR-oriented FL defense frameworks that prioritize both robustness against backdoor attacks and resilience to speckle noise, ensuring reliable performance in challenging SAR imaging conditions.

III. PROPOSED METHOD

This section introduces the backdoor defense setting in SAR-oriented FL and presents the NADAFD framework, with the system architecture illustrated in Fig. 2.

A. Problem Definition

We consider a FL system for SAR image target recognition consisting of N clients $\{C_1, C_2, \dots, C_N\}$. Each client C_i holds a local SAR dataset $D_i = \{x_j, y_j\}_{j=1}^{n_i}$, where $x_j \in \mathbb{R}^{H \times W \times C_{ch}}$ represents a SAR image, with height H , width W , and number of channels C_{ch} , and $y_j \in \{1, \dots, K\}$ is its corresponding ground-truth class label, with K being the total number of classes. The global model parameters $\theta \in \mathbb{R}^d$ are collaboratively optimized across clients following the standard FL objective [7]:

$$\min_{\theta} \mathcal{L}_{\text{global}}(\theta) = \sum_{i=1}^N \omega_i \mathbb{E}_{(x,y) \sim D_i} [\ell(f_{\theta}(x), y)], \quad (1)$$

where $\omega_i = \frac{|D_i|}{\sum_{j=1}^N |D_j|}$ denotes the aggregation weight for client C_i , and $\ell(\cdot)$ denotes the cross-entropy loss function. The term $\mathbb{E}_{(x,y) \sim D_i}$ denotes the expectation over the local data distribution, and $f_{\theta}(x)$ is the model output for image x .

Despite protecting data privacy, the FL aggregation process remains susceptible to security vulnerabilities, particularly backdoor attacks. In the presence of adversaries, M ($M < N$) clients $\{C_{k_1}, \dots, C_{k_M}\}$ may be compromised to inject backdoor patterns during local training. From the threat perspective, we assume that these compromised clients act as backdoor attackers: each malicious client C_{k_m} functions as a white-box adversary that fully controls its local training pipeline, including poisoning local samples and modifying labels, while still complying with the FL communication protocol. Benign clients adhere to the standard FL protocol, and the central server is assumed honest and non-colluding. The server cannot access any private SAR images but is permitted to maintain a small public or synthetic SAR dataset solely for defensive analysis, which does not violate privacy. These malicious clients poison a fraction of their local data, producing a poisoned dataset D_{trigger} . Samples in this dataset are triggered inputs $x_{\text{trigger}} = x \oplus T$, constructed by embedding a predefined backdoor trigger pattern T into clean data x via an embedding operation \oplus (e.g., blending or patch insertion). These triggered inputs are crafted to induce a targeted misclassification to label y_{target} , while preserving normal performance on clean samples.

Thus, the adversarial objective can be formulated as jointly optimizing the backdoor objective while preserving performance on the main task:

$$\begin{aligned} \min_{\theta} & \mathbb{E}_{(x,y) \sim D_{\text{clean}}} \ell(f_{\theta}(x), y) \\ & + \lambda_{\text{atk}} \mathbb{E}_{(x,y) \sim D_{\text{trigger}}} \ell(f_{\theta}(x_{\text{trigger}}), y_{\text{target}}), \end{aligned} \quad (2)$$

where D_{clean} represents the clean data distribution held by benign clients, and D_{trigger} represents the poisoned data distribution held by malicious clients. λ_{atk} controls the relative strength of the backdoor objective. Poisoned updates propagate through aggregation and ultimately cause persistent misclassification of triggered inputs.

In this work, we consider targeted backdoor attacks implemented through label poisoning under a realistic threat model: malicious clients have white-box access to their own model states and training hyperparameters but cannot view other clients' data or influence the server beyond submitting local updates. Both one-shot and persistent attacks are examined in our experimental settings.

B. Challenges and Motivations

Under the above threat model, although FL preserves data privacy, its defense effectiveness against backdoor attacks is significantly compromised in SAR scenarios due to three crucial factors: spectral energy bias, speckle noise interference, and adaptive attack dynamics. These SAR-specific factors create unique vulnerabilities that cannot be effectively mitigated by existing FL defense mechanisms.

1) Spectral concealment. SAR images exhibit a pronounced energy concentration in low-frequency regions due to the coherent imaging mechanism:

$$\sum_{(u,v) \in \text{Low}} |X(u,v)|^2 \gg \sum_{(u,v) \in \text{High}} |X(u,v)|^2, \quad (3)$$

where $X(u,v) = \mathcal{F}x(u,v)$ is the two-dimensional Fourier spectrum of image x , and “Low/High” denote low/high-frequency index sets.

This spectral dominance in low-frequency bands allows attackers to embed triggers within spectrally dominant but spatially inconspicuous components. Such perturbations cause minimal spatial distortion and are often overlooked by spatial-domain detection methods. This motivates the incorporation of frequency-domain analysis to capture anomalous spectral patterns, providing a complementary defense particularly relevant in SAR imagery.

2) Speckle noise masking. SAR images suffer from multiplicative speckle noise modeled by a Gamma distribution:

$$p(x; \mu, L) = \frac{L^L x^{L-1}}{\mu^L \Gamma(L)} e^{-\frac{Lx}{\mu}}, \quad x > 0, \quad (4)$$

where x represents the pixel intensity value of a SAR image, μ denotes the mean, L represents the shape parameter, and $\Gamma(L)$ indicates the Gamma function.

This multiplicative noise interacts with backdoor perturbations δ in a non-additive manner, effectively masking their spectral and spatial signatures and making triggers difficult to distinguish from benign speckle induced variations. This motivates explicitly modeling Gamma-distributed speckle during

Algorithm 1 NADAFD Framework

Require: Clients $\mathcal{C} = \{C_1, \dots, C_N\}$, global model θ^0 , rounds R , wavelet operator \mathcal{W} , trigger mask $M \leftarrow 0$, learning rate η

- 1: **for** $r = 1$ **to** R **do**
- 2: **Server broadcasts** θ^{r-1} and x_{adv} (if $r > 1$)
- 3: **for each client** $C_i \in \mathcal{C}$ **in parallel do**
- 4: // NAAT strategy:
 - 5: ▷ Generate $x_{\text{adv}} \sim \mathcal{G}(\mu, L)$
 - 6: ▷ Compute $\mathcal{L} = \ell(f(x), y) + \beta \cdot \ell(f(x_{\text{adv}}), y)$
 - 7: ▷ Update θ_i^r with spatial-channel attention
 - 8: Send $\Delta\theta_i^r$ and feedback metrics to server
- 9: **end for**
- 10: **Server executes:**
 - 11: 1. Frequency-domain trigger detection:
 - 12: **for** $C_i \in \mathcal{C}$ **do**
 - 13: $W_i^r \leftarrow \mathcal{W}(\Delta\theta_i^r)$ ▷ Apply wavelet transform
 - 14: $E_i^r \leftarrow \|W_i^r\|_F^2$ ▷ Compute energy matrix
 - 15: **end for**
 - 16: $D^r \leftarrow \max(E^r) - \min(E^r)$
 - 17: $M \leftarrow \mathbb{I}(D^r > \zeta \cdot \text{mean}(D^r))$ ▷ Update trigger mask
 - 18: 2. Generate adversarial samples:
 - 19: $M_{\text{spatial}} \leftarrow \mathcal{W}^{-1}(M)$
 - 20: $x_{\text{adv}} \leftarrow x \odot (1 + \mathcal{G}(\mu, L)) + \xi T \odot M_{\text{spatial}}$
 - 21: 3. DHAT aggregation:
 - 22: **for** $C_i \in \mathcal{C}$ **do**
 - 23: Compute H_i^r via gradient shift and prediction divergence
 - 24: $w_i^r \leftarrow \begin{cases} \exp(-\gamma H_i^r) & \text{if } H_i^r < \tau \\ 0 & \text{otherwise} \end{cases}$
 - 25: **end for**
 - 26: $\theta^r \leftarrow \sum_i \frac{w_i^r}{\sum_j w_j^r} \cdot \theta_i^r$ ▷ Weighted aggregation
 - 27: Update τ, γ, δ ▷ Dynamic parameter adjustment
 - 28: **end for**

robustness training to enhance model robustness under SAR-specific speckle noise conditions.

3) Adaptive threats. Adversaries can adapt their strategies across communication rounds [35]. The set of malicious clients at round r is defined as:

$$A^r = \{C_i \mid \delta_i^r = \lambda_i^r \cdot T_i^r\}, \quad (5)$$

where δ_i^r denotes the attack component within client C_i 's update at round r , λ_i^r represents the time-varying attack strength, and T_i^r indicates the evolving trigger pattern.

Static defense schemes cannot effectively counteract such evolving behaviors and may even amplify malicious contamination through aggregation. This motivates a dynamic client evaluation mechanism that adapts its defensive response across communication rounds to mitigate evolving attacks.

In summary, the distinctive challenges of SAR environments, specifically frequency-domain vulnerabilities, speckle-induced perturbation masking, and adaptive adversarial behaviors, which motivate an integrated design combining frequency-aware detection, speckle-consistent robustness training, and temporal adaptation, as detailed in Algorithm 1.

C. Proposed Framework

To address these challenges, we propose NADAFD as a multi-tiered federated defense framework as illustrated in Fig. 2 that integrates detection, robustness enhancement, and adaptive coordination, forming a closed-loop workflow encompassing sensing, response, feedback, adaptation, and model updates.

Step 1. Local training and gradient upload (Client). Each client C_i trains local model parameters θ_i^r on local data D_i , computes local gradients $g_i^r = \nabla_{\theta} \mathcal{L}_i^{\text{adv}}(\theta_i^r; D_i)$, and uploads them to the server.

Step 2. Spectral collaborative inversion (Server). The server aggregates gradients $\{g_i^r\}_{i=1}^N$, performs wavelet-based spectral analysis to identify anomalous spectral energy regions. Although the resulting mask is derived from parameter updates rather than the image domain, it is interpreted as a cross-client vulnerability indicator that reflects shared abnormal update directions across clients rather than exact spatial trigger locations.

Step 3. Generation and broadcasting of adversarial samples (Server \rightarrow Client). The server generates adversarial samples x_{adv} using Gamma-distributed speckle noise modeling and broadcasts them.

Step 4. Attention-enhanced robust training (Client). Clients update local models using both clean samples and adversarial samples. Two attention mechanisms, channel attention $CA(\cdot)$ and spatial attention $SA(\cdot)$, are employed to improve robustness and emphasize discriminative regions. The spatial attention prior helps clients emphasize model-vulnerable regions during adversarial training.

Step 5. Health assessment and feedback-driven aggregation (Client \leftrightarrow Server). The server computes client health scores $h_i^{(r)}$, adaptively adjusts aggregation weights $w_i^{(r)}$, and updates the global model $\theta^{(r+1)}$, while clients return state vectors to close the feedback loop. This feedback-driven mechanism enables the system to adapt aggregation behavior dynamically as attack patterns evolve, maintaining a fully closed-loop adaptive defense process. Details of each phase are provided in the following subsections.

1) *Cross-client frequency domain collaborative inversion mechanism:* In SAR data, backdoor triggers often concentrate in low-frequency subbands, making them difficult to detect via raw images or single-client gradients. To address this, we propose a frequency domain collaborative inversion (FDCI) mechanism that aggregates client gradients in the spectral domain and identifies anomalous energy patterns using wavelet-based multi-resolution analysis, which more effectively captures localized anomalies than fixed-resolution frequency transforms.

We utilize Haar wavelets as basis functions with a decomposition level $J = 3$ to balance representation resolution and computational complexity. Let $\Delta\theta_i^r$ be the model update of client C_i at round r , whose spectral representation is computed as:

$$W_i^r = \mathcal{W}(\Delta\theta_i^r), \quad E_i^r = \|W_i^r\|^2, \quad (6)$$

where $\mathcal{W}(\cdot)$ denotes the wavelet transform and E_i^r represents the energy map in the transform domain.

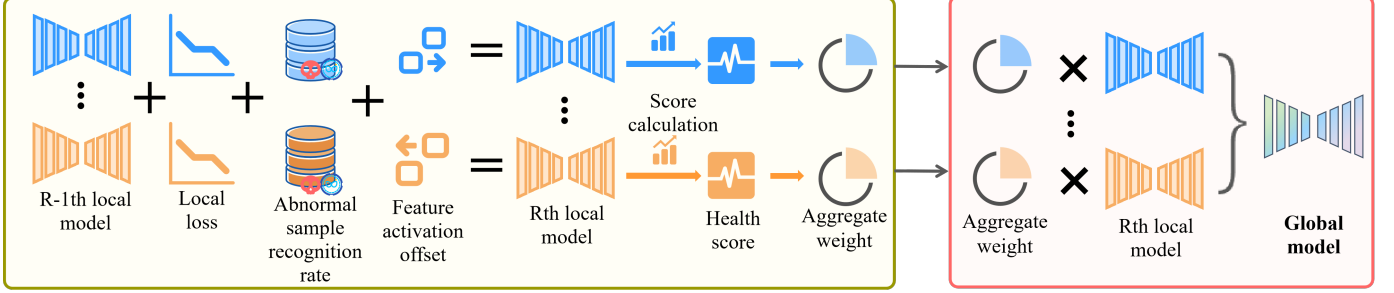


Fig. 3: The DHAT mechanism defends against poisoning attacks by evaluating client reliability and dynamically adjusting aggregation weights.

To detect spectral anomalies, the server computes a discrepancy map across clients:

$$D^r(p, q) = \max_i E_i^r(p, q) - \min_i E_i^r(p, q), \quad (7)$$

where (p, q) indicates the transform-domain location in the energy map.

Regions with significant spectral deviations are highlighted through a binary mask:

$$M(p, q) = \begin{cases} 1, & \text{if } D^r(p, q) > \zeta \cdot \text{mean}(D^r) \\ 0, & \text{otherwise} \end{cases}, \quad (8)$$

where ζ is a threshold parameter that controls detection sensitivity. The binary frequency-domain mask M is mapped into the spatial domain through $M_{\text{spatial}} = \mathcal{W}^{-1}(M)$, which subsequently guides perturbation design and anomaly filtering.

By capturing cross-client spectral inconsistencies, this approach identifies potential backdoors beyond single-client detection capabilities and leverages SAR-specific distinctive spectral characteristics, resulting in improved coordination and localization.

2) *Noise adaptive adversarial training mechanism*: Standard adversarial training typically assumes additive Gaussian noise, which fundamentally mismatches the multiplicative Gamma-distributed speckle noise present in SAR images. This mismatch reduces robustness and backdoor detection performance.

We introduce a noise-aware adversarial training (NAAT) strategy to generate adversarial examples that are aligned with SAR-specific speckle noise, leveraging frequency-domain masks to localize vulnerable regions.

The adversarial sample generation process is formally defined as:

$$x_{\text{adv}} = x \odot (1 + N_i) + \xi \cdot T \odot M_{\text{spatial}}, \quad (9)$$

where x represents the SAR image, $N_i \sim \text{Gamma}(\mu, L)$ represents Gamma-distributed noise, T indicates the trigger pattern, ξ controls the injection strength, and $M_{\text{spatial}} = \mathcal{W}^{-1}(M)$ projects spectral anomalies to the spatial domain. Here, \odot denotes element-wise multiplication.

Clients incorporate attention mechanisms during adversarial training to enhance feature focus and robustness. The combined loss is formulated as:

$$L = \ell(f(x), y) + \beta \cdot \ell(f(x_{\text{adv}}), y), \quad (10)$$

where $f(\cdot)$ is the attention-enhanced model, and β controls the weight of adversarial loss.

By incorporating SAR-specific noise characteristics into training, this mechanism improves model robustness against both natural perturbations and adversarial triggers.

3) *Dynamic health assessment and defense closed-Loop mechanism*: As attackers dynamically adjust their strategies across rounds, static aggregation becomes ineffective, allowing evolving threats to evade detection. Leveraging FDCI's anomaly masks and NAAT's robustness feedback, the dynamic health assessment (DHAT) module provides the necessary behavioral insight to counteract these evolving threats.

We adopt a feedback-driven mechanism that adjusts aggregation by evaluating client behavior over time, as illustrated in Fig. 3.

Health scores are computed as:

$$H_i^r = \gamma \cdot \|\Delta\theta_i^r - \Delta\theta_i^{r-1}\|_2 + \delta \cdot D_{\text{KL}}(f_i^r, f_i^{r-1}), \quad (11)$$

where γ and δ are weights balancing the two score components, $\Delta\theta_i^r$ denotes the parameter update at round r , and D_{KL} measures output distribution shifts between consecutive rounds.

Based on H_i^r , aggregation weights are adjusted as:

$$w_i^r = \begin{cases} \exp(-H_i^r) \cdot c, & H_i^r < \tau \\ 0, & H_i^r \geq \tau \end{cases}, \quad w_i^r \leftarrow \frac{w_i^r}{\sum_j w_j^r}, \quad (12)$$

where the threshold τ is dynamically adjusted to counter evolving attacker behaviors.

To suppress anomalous updates, NADAFD employs frequency-domain masks M to detect suspicious regions and spatial-domain versions M_{spatial} to guide selective suppression during aggregation. The framework further monitors client states through metrics such as prediction shifts and adversarial loss variance, enabling dynamic adjustment of thresholds (ζ, γ, δ) and perturbation strength (ξ) for fine-grained control. This forms a closed-loop defense cycle that enables dynamic adaptation, where suppression effectiveness informs iterative refinement of defense parameters and client trust is dynamically reassessed based on model contribution, ensuring continuous optimization of the defense strategy.

D. Convergence Analysis

For clarity of exposition, we analyze convergence under the standard data-proportion aggregation weights $\{\omega_i\}$ and absorb

the deviations induced by DHAT into the bias term defined below. The global objective is:

$$\min_{\theta \in \mathbb{R}^d} L_{\text{global}}(\theta) := \sum_{i=1}^N \omega_i L_i^{\text{adv}}(\theta), \quad (13)$$

where $\omega_i = \frac{|D_i|}{\sum_{j=1}^N |D_j|}$ represents the data proportion weight for client C_i .

The local adversarial loss on client C_i is given by

$$L_i^{\text{adv}}(\theta) = \mathbb{E}_{(x,y) \sim D_i} \left[\ell(f_\theta(x), y) + \beta \cdot \ell(f_\theta(x_{\text{adv}}), y) \right], \quad (14)$$

where x_{adv} is generated using NAAT with Gamma-distributed noise and mask M_{spatial} , as defined in Eq. (9). The composite weight β modulates adversarial strength and is dynamically tuned by DHAT.

To analyze the convergence of NADAFD, we first make the following assumptions.

Assumption 1. All local loss functions are L -smooth, i.e., for any $\theta, \theta' \in \mathbb{R}^d$:

$$\|\nabla L_i^{\text{adv}}(\theta) - \nabla L_i^{\text{adv}}(\theta')\| \leq L \|\theta - \theta'\|. \quad (15)$$

Assumption 2. Local gradients form unbiased estimators with bounded variance, where σ^2 serves as a constant such that for any θ :

$$\mathbb{E}_i [\nabla L_i^{\text{adv}}(\theta)] = \nabla L_{\text{global}}(\theta), \quad (16)$$

and

$$\mathbb{E} \|\nabla L_i^{\text{adv}}(\theta) - \nabla L_{\text{global}}(\theta)\|^2 \leq \sigma^2. \quad (17)$$

Assumption 3. The global adversarial objective L_{global} admits a weakly convex [36] and gradient-dominant surrogate [37]. Specifically, there exists $\mu > 0$ such that for any $\theta, \theta' \in \mathbb{R}^d$,

$$L_{\text{global}}(\theta') \geq L_{\text{global}}(\theta) + \langle \nabla L_{\text{global}}(\theta), \theta' - \theta \rangle - \frac{\mu}{2} \|\theta' - \theta\|^2, \quad (18)$$

and

$$\frac{1}{2} \|\nabla L_{\text{global}}(\theta)\|^2 \geq \mu (L_{\text{global}}(\theta) - L^*). \quad (19)$$

Although the practical model is highly non-convex due to CNN layers, attention modules, and adversarial perturbations, direct analysis of the full objective is intractable. Following standard practice in federated optimization, we approximate it with a weakly convex and gradient-dominant surrogate, where weak convexity bounds negative curvature such that $L_{\text{global}}(\theta) + \frac{\mu}{2} \|\theta\|^2$ is convex [36], and gradient dominance links the gradient norm to function suboptimality [37]. This approximation preserves descent-type convergence behavior without imposing strong convexity.

In training round r , each client employs the current global model θ^r to perform τ local gradient descent steps with learning rate η , generating the local model update as follows:

$$\theta_i^{r+1} = \theta^r - \eta \sum_{t=0}^{\tau-1} \nabla L_i^{\text{adv}}(\theta_i^{r,t}), \quad (20)$$

where $\theta_i^{r,0} = \theta^r$ and $\theta_i^{r,t+1} = \theta_i^{r,t} - \eta \nabla L_i^{\text{adv}}(\theta_i^{r,t})$. During the aggregation phase, the server performs global aggregation using the data-proportion weights ω_i :

$$\theta^{r+1} = \sum_{i=1}^N \omega_i \theta_i^{r+1}. \quad (21)$$

Let the average local gradient be

$$\bar{g}^r = \nabla L_{\text{global}}(\theta^r) + \delta^r, \quad (22)$$

where δ^r denotes the accumulated bias introduced by local multi-step updates, dynamic reweighting, and noise perturbations. With FDCI and NAAT, this bias can be decomposed as

$$\delta^r = (1 - \kappa) \delta_T^r + \delta_N^r, \quad (23)$$

where δ_T^r is the trigger-induced bias, δ_N^r is noise-induced, and κ is the suppression rate of FDCI masks.

Using L -smoothness of L_{global} and standard arguments for gradient descent with biased gradients, one can show that

$$\mathbb{E}[L_{\text{global}}(\theta^{r+1})] \leq \mathbb{E}[L_{\text{global}}(\theta^r)] + L\eta^2 \mathbb{E}\|\delta^r\|^2 - (\eta - L\eta^2) \mathbb{E}\|\nabla L_{\text{global}}(\theta^r)\|^2. \quad (24)$$

Combining this with the gradient-dominance surrogate in Assumption 3 yields

$$\mathbb{E}[L_{\text{global}}(\theta^{r+1}) - L^*] \leq \rho \cdot \mathbb{E}[L_{\text{global}}(\theta^r) - L^*] + L\eta^2 \mathbb{E}\|\delta^r\|^2, \quad (25)$$

where $\rho = 1 - 2\eta\mu + 2L\eta^2\mu$. If $\eta < \frac{1}{2L}$, then $\rho < 1$, so the expected suboptimality decays geometrically up to the bias term.

From the decomposition of δ^r we have

$$\mathbb{E}\|\delta^r\|^2 \leq (1 - \kappa)^2 \mathbb{E}\|\delta_T^r\|^2 + \mathbb{E}\|\delta_N^r\|^2. \quad (26)$$

Assuming that $\sup_r \mathbb{E}\|\delta_T^r\|^2$ and $\sup_r \mathbb{E}\|\delta_N^r\|^2$ are finite, recursively applying the above inequality gives the final error bound

$$\begin{aligned} \mathbb{E}[L_{\text{global}}(\theta^r) - L^*] &\leq \frac{L\eta^2}{1 - \rho} (1 - \kappa)^2 \sup_r \mathbb{E}\|\delta_T^r\|^2 \\ &\quad + \frac{L\eta^2}{1 - \rho} \sup_r \mathbb{E}\|\delta_N^r\|^2 \\ &\quad + \rho^r (L_{\text{global}}(\theta^0) - L^*). \end{aligned} \quad (27)$$

This shows that as $\kappa \rightarrow 1$ and noise effects are mitigated by NAAT, the impact of backdoors and speckle noise vanishes in the bias term, and NADAFD converges geometrically under adaptive weighting by DHAT in the sense of the above bound.

IV. EXPERIMENT

A. Experimental Settings

1) *Datasets and Evaluation Protocol:* We evaluate the proposed method on two widely used SAR target recognition benchmarks: MSTAR [38] and OpenSARShip [39]. A detailed summary of dataset statistics is reported in Table I, and representative examples are shown in Fig. 4 and Fig. 5.

For evaluation, we report the main-task classification accuracy on clean test samples and the backdoor attack success rate on triggered inputs (denoted as ACC and ASR, respectively) [40], [41]. To better capture performance under label imbalance, we additionally report the macro-averaged F1

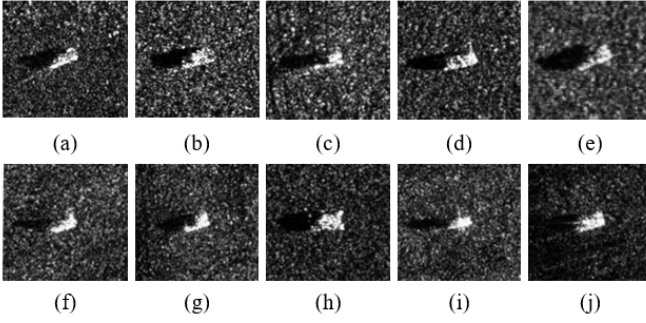


Fig. 4: The MSTAR dataset includes ten target categories with SAR images. (a) 2S1, (b) BMP2, (c) BRDM2, (d) BTR60, (e) BTR70, (f) D7, (g) T62, (h) T72, (i) ZIL131, (j) ZSU234.

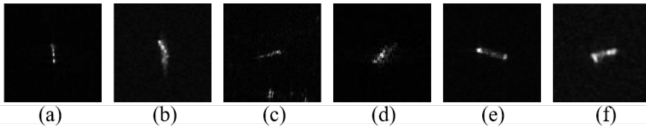


Fig. 5: The OpenSARShip dataset includes six target categories with SAR images. (a) Bulk Carrier, (b) Container Ship, (c) Tanker, (d) Cargo Ship, (e) Fishing, (f) General Cargo.

score [42] in a representative non-IID configuration. To assess system overhead, we report the per-round client/server latency (s/round).

2) *Federated Learnin Setting*: We consider a cross-silo FL scenario with $K = 10$ clients. In each communication round, the server uniformly samples a fraction $C = 0.5$ of clients and aggregates their local updates. To simulate realistic data heterogeneity, client datasets follow a label-skewed non-IID partition generated by a Dirichlet distribution $\text{Dir}_N(\alpha)$, where $\alpha \in 1.0, 0.5, 0.1, 0.05$. Smaller α values correspond to more severe label skew. Each client performs local optimization using SGD with an initial learning rate of 0.02, momentum 0.9, weight decay 10^{-4} , batch size 32, and $E = 2$ local epochs per round, with a cosine decay schedule over the global rounds. The total number of communication rounds is fixed to $R = 200$, which is sufficient for stable convergence. To avoid degenerate cases, we enforce a minimum number of samples per client during data partitioning. All clients adopt a lightweight convolutional backbone equipped with spatial and channel attention. Batch normalization statistics remain local to each client, and mixed-precision training is enabled when supported. For NADAFD, FDCI employs Haar wavelets with decomposition level $J = 3$. NAAT uses Gamma-distributed speckle noise with an equivalent number of looks $L = 3$, perturbation strength $\xi = 0.05$, and adversarial loss weight $\beta = 0.5$. The health-based aggregation threshold is set to $\tau = \text{P95}$.

3) *Threat Model and Baseline Methods*: We consider a strong and practical backdoor threat model in which a subset of clients is malicious. Each malicious client poisons its local data by embedding a stealthy 3×3 high-intensity scatterer trigger into the low-frequency spectrum of SAR images, guided

TABLE I
TRAINING AND TEST DATA DISTRIBUTION OF DATASETS

Dataset	Target Category	Training	Test
MSTAR	2S1	299	273
	BMP2	233	195
	BRDM2	298	274
	BTR60	256	195
	BTR70	233	196
	D7	299	274
	T62	299	274
	T72	299	274
	ZIL131	299	274
	ZSU234	299	274
OpenSARShip	Bulk Carrier	200	475
	Container Ship	200	811
	Tanker	200	354
	Cargo Ship	200	557
	Fishing	200	121
	General Cargo	200	165

TABLE II
PERFORMANCE UNDER VARYING ATTACK PARAMETERS IN THE NON-IID SETTING (MSTAR, DIRICHLET $\alpha = 0.5$).

Method	Varying poisoning ratio			Varying malicious clients		
	10%	20%	30%	1/10	2/10	3/10
ACC (%)						
FedAvg [7]	91.21	88.73	85.34	92.81	88.61	83.54
Krum [32]	90.53	87.89	85.14	91.53	87.34	83.94
Median [43]	90.97	88.13	85.58	91.85	88.05	84.54
FedID [41]	91.81	89.65	87.14	92.33	92.45	86.22
Lockdown [44]	91.53	89.17	86.86	92.13	89.17	85.94
EH-AT [45]	91.66	89.25	86.74	92.21	89.01	85.54
FSBA [40]	91.01	88.65	86.02	91.73	88.33	84.82
RRPD [46]	91.37	91.45	86.42	92.01	88.73	85.14
NADAFD (Ours)	93.21	90.97	88.93	93.41	93.53	88.37
ASR (%)						
FedAvg [7]	88.50	95.70	97.30	85.20	95.60	98.60
Krum [32]	42.10	55.70	63.00	40.50	52.30	69.40
Median [43]	36.80	49.10	57.80	35.20	46.80	65.70
FedID [41]	12.30	18.70	25.40	10.80	18.50	27.30
Lockdown [44]	10.70	16.20	22.90	9.40	16.10	24.80
EH-AT [45]	14.20	24.30	31.80	13.00	23.50	33.70
FSBA [40]	21.20	31.40	38.60	19.80	30.20	41.50
RRPD [46]	17.80	28.10	35.40	16.50	27.50	38.90
NADAFD (Ours)	3.20	5.70	8.90	2.80	5.60	10.20

by a frequency-domain binary mask to ensure imperceptibility in both spatial and spectral domains [47]. Triggered samples are forced to a fixed target label. Two attack modes are evaluated: a single-shot attack [29], where poisoning occurs in one communication round, and a persistent attack [35], where poisoning is repeated in every round. The number of malicious clients varies from 1 to 5 (i.e., 10%–50% of all clients), and the local poisoning ratio ranges from 10% to 50%. All results are averaged over multiple source–target class pairs.

We compare NADAFD with the standard FL baseline FedAvg [7], Byzantine-robust aggregation methods Krum [32] and Median [43], and recent federated backdoor defenses FedID [41] and Lockdown [44]. In addition, SAR- and spectrum-oriented defenses, including EH-AT [45], FSBA [40], and RRPD [46], are adapted to the federated SAR setting for fair comparison. We also evaluate ablated variants of NADAFD by removing FDCI, NAAT, or DHAT to isolate the contribution

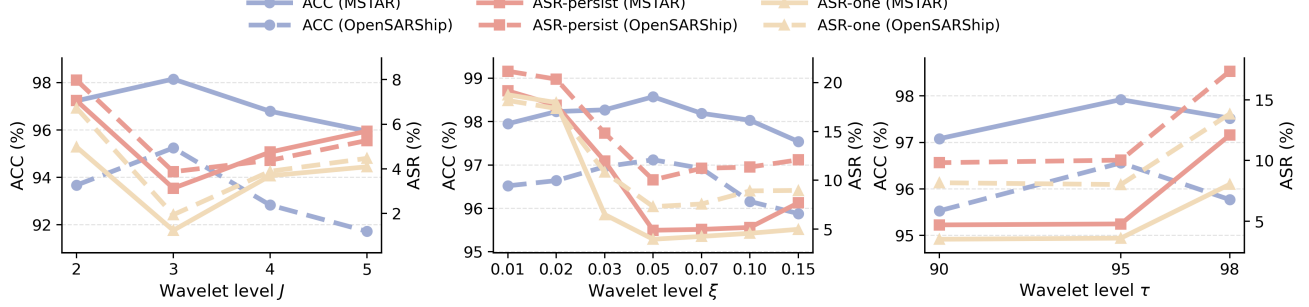


Fig. 6: Effect of wavelet levels J , ξ , and τ on ACC and ASR for MSTAR and OpenSARShip datasets.

TABLE III
ACC (%) UNDER DIFFERENT MALICIOUS-CLIENT RATIOS ON MSTAR AND OPENSARSHIP

Baselines	MSTAR										OpenSARShip											
	Clean	One-shot (mal.%)					Persistent (mal.%)					Clean	One-shot (mal.%)					Persistent (mal.%)				
		10	20	30	40	50	10	20	30	40	50		10	20	30	40	50	10	20	30	40	50
FedAvg [7]	94.97	94.69	94.09	92.13	91.05	89.97	92.09	90.85	89.41	88.05	86.74	92.81	91.85	91.25	90.53	89.93	89.21	90.93	89.77	88.45	87.14	85.98
Krum [32]	95.13	95.01	94.67	93.05	91.91	90.17	91.57	90.49	89.13	87.85	86.58	91.21	90.33	89.81	89.37	88.81	88.37	90.21	89.33	88.05	86.82	85.66
Median [43]	95.05	94.85	94.41	92.65	92.17	90.09	91.81	90.73	89.45	88.05	86.74	91.61	90.81	90.37	89.81	89.33	88.81	90.73	89.65	88.33	87.06	85.94
FedID [41]	94.93	94.89	94.45	93.49	92.05	90.97	92.73	91.97	90.69	89.57	88.49	92.33	91.73	91.33	90.93	90.57	90.13	91.41	90.53	89.41	88.37	87.34
Lockdown [44]	94.89	94.81	94.41	93.45	91.77	90.93	92.93	92.13	90.85	89.61	88.61	92.13	91.45	91.01	90.65	90.21	89.85	91.33	90.77	89.61	88.57	87.42
EH-AT [45]	95.05	95.01	94.49	93.53	92.17	90.57	93.25	92.57	91.45	90.29	89.09	92.21	91.61	91.21	90.73	90.37	89.81	91.41	90.93	89.85	88.73	87.65
FSBA [40]	94.93	94.89	94.29	92.61	91.69	90.13	91.65	90.65	89.21	87.85	86.46	91.41	90.53	90.05	89.50	89.01	88.53	90.37	89.45	88.13	86.94	85.78
RRPD [46]	95.01	94.97	94.53	93.57	92.13	90.65	93.13	92.45	91.33	90.17	89.05	91.93	91.21	90.73	90.25	89.73	89.21	91.25	90.77	89.65	88.57	87.42
NADAFD (Ours)	95.05	95.09	94.81	93.77	92.53	91.01	93.45	92.93	92.21	91.37	90.65	93.09	92.37	92.01	91.61	91.37	90.97	92.01	91.33	90.45	89.57	88.77

of each component.

B. Analysis of NADAFD Parameters

We analyze the impact of NADAFD core hyperparameters on robustness and model utility under on both MSTAR and OpenSARShip datasets with persistent backdoor attacks, Dirichlet non-IID partition $\alpha = 0.5$, a malicious-client ratio of 30%, and a local poisoning ratio of 30%.

1) *Impact of Wavelet Decomposition Level J :* We study the effect of the wavelet decomposition level $J \in \{2, 3, 4, 5\}$ on NADAFD. As shown in Fig. 6, we observe a pronounced U-shaped trend in ASR as J varies. A shallow decomposition (e.g., $J=2$) fails to sufficiently isolate low-frequency trigger energy, resulting in high ASR (around 8–10% on both datasets), while overly deep decomposition ($J \geq 4$) introduces high-frequency artifacts that again degrade detection performance. We find that $J=3$ consistently yields the lowest ASR (below 3%) and the highest ACC across both datasets and attack settings, indicating that it offers the best trade-off between spectral resolution and stability. Therefore, we adopt $J^*=3$ as the default configuration in all subsequent experiments.

2) *Impact of Adversarial Perturbation Strength ξ :* We evaluate the impact of adversarial perturbation strength by varying $\xi \in \{0.01, 0.02, 0.03, 0.05, 0.07, 0.10, 0.15\}$. As shown in Fig. 6, we find that small perturbations ($\xi \leq 0.02$) are insufficient to expose backdoor vulnerabilities, leading to high ASR (around 15%). Increasing ξ significantly improves robustness, and performance stabilizes near $\xi=0.05$, where ASR is minimized (around 3%) and ACC remains high. Larger

perturbations (e.g., $\xi \geq 0.10$) provide diminishing returns and may slightly destabilize training. We therefore adopt $\xi^*=0.05$ as the default value.

3) *Impact of Aggregation Threshold τ :* We investigate percentile-based aggregation thresholds $\tau \in \{P98, P95, P90\}$ for client pruning. As illustrated in Fig. 6, we observe that lowering the percentile threshold from P98 to P95 substantially lowers ASR (down to around 3–4%) while keeping ACC largely unchanged. Further tightening the threshold to P90 brings only marginal additional gains (typically below 0.5 percentage points) but introduces higher variance due to more aggressive pruning. We find that P95 strikes the most stable balance between robustness and model ACC and therefore adopt $\tau^*=P95$ as the default setting in subsequent experiments.

4) *Impact of Local Poisoning Ratio and Malicious Clients:* Beyond the core hyperparameters, we further analyze NADAFD under varying attack intensities under the standard non-IID configuration (Dirichlet $\alpha = 0.5$): local poisoning ratio and malicious-client fraction. As summarized in Table II, stronger attacks consistently reduce ACC and increase ASR across all methods. Nevertheless, NADAFD achieves the highest ACC and lowest ASR across all configurations. The ASR growth for NADAFD is significantly slower as attack strength increases than that of existing defenses, showing that the proposed frequency-domain gating and NAAT model suppress backdoor amplification under strong attacks.

TABLE IV

ASR (%) UNDER ONE-SHOT AND PERSISTENT ATTACKS WITH AN EXPLICIT IID BASELINE AND NON-IID (DIRICHLET α)

Baselines	MSTAR										OpenSARShip									
	One-shot					Persistent					One-shot					Persistent				
	IID	1	0.5	0.1	0.05	IID	1	0.5	0.1	0.05	IID	1	0.5	0.1	0.05	IID	1	0.5	0.1	0.05
FedAvg [7]	92.24	94.04	95.61	97.62	98.21	96.46	97.80	98.34	99.10	99.37	93.54	95.56	96.23	97.85	98.35	97.26	98.52	98.97	99.46	99.55
Krum [32]	45.42	50.31	52.15	56.37	57.26	62.56	68.16	70.72	75.83	77.44	47.09	52.74	54.62	59.19	60.27	65.38	71.88	74.04	78.12	80.04
Median [43]	39.24	44.53	46.46	50.85	52.42	56.55	62.74	65.07	69.46	71.12	40.81	47.31	49.28	53.81	55.65	59.37	66.01	68.25	72.56	74.44
FedID [41]	15.39	17.91	18.78	20.65	21.30	24.78	28.65	29.91	32.57	33.74	16.91	19.65	20.61	22.78	23.43	27.04	31.13	32.39	35.13	36.48
Lockdown [44]	12.65	15.35	16.22	18.04	18.83	21.22	25.13	26.48	29.17	30.26	14.35	17.13	18.04	20.09	20.87	23.61	27.78	29.09	32.04	33.26
EH-AT [45]	14.17	16.96	17.91	19.83	20.57	22.96	27.43	28.74	31.65	32.91	15.87	18.91	19.83	21.96	22.65	25.43	29.87	31.26	34.57	35.87
FSBA [40]	22.17	26.43	27.87	31.13	31.96	35.35	40.83	42.56	46.37	47.71	24.35	29.13	30.65	34.13	35.26	38.74	44.13	45.83	49.64	50.94
RRPD [46]	18.48	22.26	23.57	26.43	27.26	30.17	35.52	37.43	41.35	42.83	20.96	25.22	26.48	29.35	30.48	33.17	38.74	40.39	44.44	45.83
NADAFD	4.17	5.26	5.65	6.57	6.91	7.48	8.87	9.26	9.91	9.96	5.35	7.04	7.43	8.65	8.96	8.74	10.57	11.22	12.52	13.17

TABLE V

MACRO-F1 (%) ON MSTAR AND OPENSARSHIP UNDER PERSISTENT ATTACKS (NON-IID, $\alpha = 0.5$, 30% MALICIOUS, 30% POISONING).

Method	MSTAR	OpenSARShip
FedAvg [7]	88.53	83.02
Krum [32]	88.33	83.18
Median [43]	88.57	83.26
FedID [41]	89.85	84.22
Lockdown [44]	90.41	84.34
EH-AT [45]	90.77	85.82
FSBA [40]	88.29	84.58
RRPD [46]	90.73	85.30
NADAFD (Ours)	91.53	86.94

C. Performance Comparison

1) *Main Task Accuracy*: Table III shows that all methods achieve similar clean ACC on MSTAR and OpenSARShip, indicating comparable utility on benign data. Under one-shot and persistent attacks, however, NADAFD consistently maintains the highest ACC, and the margin widens as the malicious-client ratio increases. This superiority mainly comes from NADAFD’s ability to filter low-frequency spectral anomalies before aggregation, which preserves benign non-IID variations while suppressing poisoned gradients. In contrast, Krum and Median tend to oversuppress heterogeneity, whereas FedID and Lockdown are designed for natural-image FL and do not account for SAR’s multiplicative Gamma speckle. SAR-specific components in NADAFD, frequency gating plus noise-aware adversarial exposure, enable the model to separate genuine backscatter patterns from trigger-like spectra. Overall, NADAFD delivers the strongest clean-task performance across all attack intensities.

2) *Defense Effectiveness*: As shown in Table IV, NADAFD achieves the lowest ASR across MSTAR and OpenSARShip under both IID and non-IID settings. FedAvg remains highly vulnerable (persistent ASR often $>95\%$), while Krum, Median, FedID, and Lockdown reduce ASR only partially, especially under persistent non-IID conditions. FSBA, EH-AT, and RRPD improve robustness but struggle with low-frequency triggers in Gamma-speckle environments, leaving substantial residual ASR. In contrast, NADAFD keeps ASR below 10% on MSTAR across all α and in the low teens on OpenSARShip. It achieves this by jointly suppressing spectral trigger

energy, exposing the model to speckle-consistent adversarial perturbations, and dynamically reweighting suspicious clients. These coordinated mechanisms prevent trigger accumulation and provide stable defense.

3) *Additional Metrics under Class Imbalance*: To better capture performance under class imbalance, we further examine the macro-averaged F1 score (macro-F1) under the same representative non-IID configuration ($\alpha = 0.5$, 30% malicious clients, 30% poisoning), complementing the ACC results reported in Table III.

On MSTAR, whose class distribution is relatively balanced, macro-F1 remains close to ACC for most methods (cf. Table III and Table V), with NADAFD achieving the highest score, confirming its strong per-class performance.

On OpenSARShip, which suffers from stronger class imbalance, many baselines show substantially lower macro-F1 than ACC in Table III, indicating degraded detection of minority categories. NADAFD maintains high macro-F1 together with high ACC, demonstrating balanced per-class performance even under persistent attacks and non-IID distributions.

D. Ablation and Visualization

1) *Component Ablation*: We conduct an ablation study using three controlled variants of NADAFD, as summarized in Table VI: removing FDCI, NAAT, or DHAT.

As shown in Table VI, removing FDCI yields the largest increase in ASR under both IID and non-IID settings. Without cross-client frequency analysis, the server cannot isolate low-frequency anomalous energy where SAR triggers typically reside. As a result, backdoor cues easily blend into natural speckle fluctuations and become difficult to detect. This forces the system to rely only on spatial cues, which are unreliable under multiplicative Gamma noise. Removing NAAT leads to moderate ASR increases, especially in non-IID settings. Without Gamma-consistent adversarial samples and mask-guided perturbations, the feature extractor is not explicitly exposed to speckle-induced distortions, weakening its ability to separate authentic SAR scattering patterns from trigger-like artifacts. The absence of DHAT has the smallest effect in one-shot attacks but significantly harms robustness under persistent attacks. Without dynamic reweighting, malicious clients retain stable aggregation influence, enabling gradual contamination

TABLE VI

ABLATION OF NADAFD ON **MSTAR** AND **OPEN SARSHIP** UNDER IID AND non-IID (DIRICHLET, $\alpha = 0.5$). LOWER ASR IS BETTER.

Methods	MSTAR (IID)			MSTAR (non-IID, $\alpha = 0.5$)			OpenSARShip (IID)			OpenSARShip (non-IID, $\alpha = 0.5$)		
	ACC _{clean}	ASR _{one}	ASR _{pers}	ACC _{clean}	ASR _{one}	ASR _{pers}	ACC _{clean}	ASR _{one}	ASR _{pers}	ACC _{clean}	ASR _{one}	ASR _{pers}
NADAFD (Full)	95.05	4.13	7.46	94.05	5.66	9.27	93.09	5.36	8.74	92.01	7.41	11.23
–FDCI	93.40	13.91	12.80	92.02	17.34	25.27	91.35	19.54	18.10	89.02	22.87	33.21
–NAAT	94.10	8.24	13.02	93.11	10.41	16.37	91.72	11.63	18.33	90.47	13.92	22.18
–DHAT	94.32	7.83	11.57	93.03	9.86	14.92	91.29	10.94	16.02	90.11	13.44	21.37

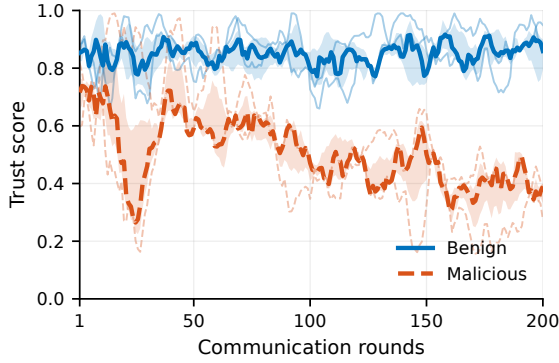


Fig. 7: Client trust indicator under a persistent backdoor attack (representative run).

of the global model over rounds, which is reflected in sharply elevated ASR in the persistent regime.

Overall, the full NADAFD model consistently achieves the lowest ASR and highest ACC, confirming the complementary roles of its components: FDCI provides reliable trigger localization in frequency space, NAAT equips the model with robustness to SAR-specific Gamma speckle, and DHAT adaptively suppresses evolving malicious behavior across rounds. Together, these modules form a unified and resilient defense for federated SAR target recognition.

2) *Visualization of Client Health Trajectories*: To complement the quantitative ablation in Table VI, we illustrate the temporal evolution of client health under a representative persistent backdoor attack. As shown in Fig. 7, benign clients (blue) remain in a high-health band, whereas malicious clients (red) stay in a distinctly lower band throughout training, providing a stable signal for aggregation.

Health-guided reweighting in DHAT progressively down-weights suspicious low-health updates while preserving benign contributions, supporting stable clean-task performance. This separation suggests that DHAT can track evolving client behaviors over rounds rather than relying on single-round anomalies.

E. Robustness under Gamma-Distributed Speckle Noise

We further evaluate robustness under SAR-specific multiplicative speckle noise modeled by a Gamma distribution, parameterized by the equivalent number of looks (ENL) $L \in \{8, 4, 2, 1\}$. We measure robustness accuracy (RA) on noisy-but-clean test samples in the presence of a backdoor attacker, and summarize RA-ENL curves by AUC-RA.

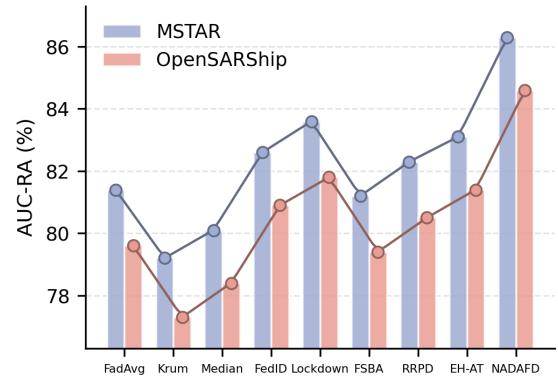


Fig. 8: AUC-RA under Gamma-distributed speckle noise (higher is better). Each bar shows the normalized trapezoidal area of the RA-ENL curve over $L \in \{8, 4, 2, 1\}$.

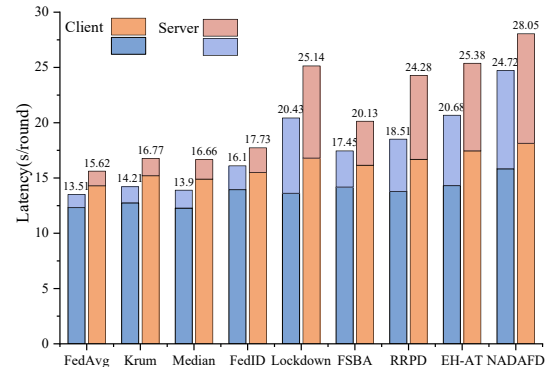


Fig. 9: Per-round client/server latency under Dirichlet non-IID ($\alpha = 0.5$) with 30% malicious clients and 30% poisoning. Left/right bars per method correspond to MSTAR/OpenSARShip, with totals (s/round) annotated above.

Fig. 8 reports AUC-RA for all methods on MSTAR and OpenSARShip. As L decreases, baselines show clear robustness degradation under intensified speckle, whereas NADAFD consistently achieves the highest AUC-RA on both datasets, indicating stronger speckle-aware robustness.

F. Computation and Communication Overhead

We evaluate the system overhead of all methods under the standard non-IID setting (Dirichlet $\alpha = 0.5$) with 30% malicious clients and a 30% poisoning ratio on both MSTAR and OpenSARShip. Fig. 9 reports the per-round client/server latency (s/round). Lightweight baselines

(FedAvg/Krum/Median) incur the lowest client-side latency, whereas NADAFD introduces moderate additional client overhead due primarily to the FDCI analysis and NAAT adversarial sample generation. On the server side, defenses with heavier spectral processing exhibit larger latency, while NADAFD remains practical by distributing its extra computation between client and server. Overall, NADAFD achieves a favorable robustness-overhead trade-off, with consistent gains in defense effectiveness at a moderate additional latency cost.

V. CONCLUSION

In this paper, we present NADAFD, a robust framework that advances trustworthy distributed intelligence for SAR-based Smart-Earth applications under backdoor attacks. By integrating FDCI for wavelet-domain inspection, NAAT for speckle-aware feature refinement, and DHAT for dynamic client reweighting, NADAFD effectively mitigates spectral trigger concealment, noise masking, and evolving adversarial behaviors. Experiments on MSTAR and OpenSARShip validate that our approach ensures high-fidelity recognition and resilience, pivotal for securing ambient intelligence systems. Future work will focus on optimizing computational efficiency for resource-constrained IoT-CI nodes.

REFERENCES

- [1] A. Moreira, P. Prats-Iraola, M. Younis, G. Krieger, I. Hajnsek, and K. P. Papathanassiou, “A tutorial on synthetic aperture radar,” *IEEE Geosci. Remote Sens. Mag.*, vol. 1, no. 1, pp. 6–43, 2013.
- [2] H.-N. Wei, G.-Q. Zeng, K.-D. Lu, G.-G. Geng, and J. Weng, “MoAR-CNN: Multi-objective adversarially robust convolutional neural network for SAR image classification,” *IEEE Trans. Emerg. Topics Comput. Intell.*, vol. 9, no. 1, pp. 57–74, 2025.
- [3] X. Zhang, T. Zhang, G. Wang, P. Zhu, X. Tang, X. Jia, and L. Jiao, “Remote sensing object detection meets deep learning: A meta-review of challenges and advances,” *IEEE Geosci. Remote Sens. Mag.*, vol. 11, no. 4, pp. 8–44, 2023.
- [4] G. Fracastoro, E. Magli, G. Poggi, G. Scarpa, D. Valsesia, and L. Verdoliva, “Deep learning methods for synthetic aperture radar image despeckling: An overview of trends and perspectives,” *IEEE Geosci. Remote Sens. Mag.*, vol. 9, no. 2, pp. 29–51, 2021.
- [5] W. Li, W. Yang, Y. Hou, L. Liu, Y. Liu, and X. Li, “SARATR-X: Toward building a foundation model for SAR target recognition,” *IEEE Trans. Image Process.*, vol. 34, pp. 869–884, 2025.
- [6] D. Li, W. Lin, W. Wu, H. Zhang, and X.-M. Wang, “Synflowfl: A dynamic synaptic flow framework for efficient, personalized federated learning,” *IEEE Trans. Emerg. Topics Comput. Intell.*, vol. 9, no. 5, pp. 3426–3440, 2025.
- [7] B. McMahan, E. Moore, D. Ramage, S. Hampson, and B. A. y. Arcas, “Communication-efficient learning of deep networks from decentralized data,” in *Proc. Int. Conf. Artif. Intell. Stat. (AISTATS)*, vol. 54, 2017, pp. 1273–1282.
- [8] Y. Zhao, L. Zhao, Z. Liu, D. Hu, G. Kuang, and L. Liu, “Attentional feature refinement and alignment network for aircraft detection in SAR imagery,” *IEEE Trans. Geosci. Remote Sens.*, vol. 60, pp. 1–16, 2022.
- [9] Y. Li, Z. Guo, N. Yang, H. Chen, D. Yuan, and W. Ding, “Threats and defenses in the federated learning life cycle: A comprehensive survey and challenges,” *IEEE Trans. Neural Netw. Learn. Syst.*, vol. 36, no. 9, pp. 15 643–15 663, 2025.
- [10] N. Dräger, Y. Xu, and P. Ghamisi, “Backdoor attacks for remote sensing data with wavelet transform,” *IEEE Trans. Geosci. Remote Sens.*, vol. 61, pp. 1–15, 2023.
- [11] S. Zheng, D. Han, C. Lu, C. Hou, Y. Han, X. Hao, and C. Zhang, “Transferable targeted adversarial attack on synthetic aperture radar (SAR) image recognition,” *Remote Sens.*, vol. 17, no. 1, p. 146, 2025.
- [12] B. Wang, Y. Yao, S. Shan, H. Li, B. Viswanath, H. Zheng, and B. Y. Zhao, “Neural cleanse: Identifying and mitigating backdoor attacks in neural networks,” in *Proc. IEEE Symp. Secur. Priv.*, 2019, pp. 707–723.
- [13] M. Fang, X. Cao, J. Jia, and N. Gong, “Local model poisoning attacks to Byzantine-Robust federated learning,” in *USENIX Secur. Symp.*, 2020, pp. 1605–1622.
- [14] X.-K. Cao, M.-S. Chen, C.-D. Wang, J.-H. Lai, Q. Huang, and C. L. P. Chen, “Dynamic secure multi-broad network for privacy preserving of streaming data,” *IEEE Trans. Emerg. Topics Comput. Intell.*, vol. 8, no. 4, pp. 3152–3165, 2024.
- [15] P. Singh, A. Shankar, and M. Diwakar, “Review on nontraditional perspectives of synthetic aperture radar image despeckling,” *J. Electron. Imaging*, vol. 32, no. 2, p. 021609, 2023.
- [16] V. Gaya, E. Dalsasso, L. Denis, F. Tupin, B. Pinel-Puysségur, and C. Guérin, “Self-supervised learning of multi-modal cooperation for SAR despeckling,” in *Proc. IEEE Int. Geosci. Remote Sens. Symp. (IGARSS)*, 2024, pp. 2180–2183.
- [17] P. Lang, X. Fu, J. Dong, H. Yang, J. Yin, J. Yang, and M. Martorella, “Recent advances in deep-learning-based SAR image target detection and recognition,” *IEEE J. Sel. Top. Appl. Earth Obs. Remote Sens.*, vol. 18, pp. 6884–6915, 2025.
- [18] Z. Wen, J. Liu, Z. Liu, S. Li, and Q. Pan, “Contrastive feature disentangling for partial aspect angles SAR noncooperative target recognition,” *IEEE Trans. Geosci. Remote Sens.*, vol. 61, pp. 1–15, 2023.
- [19] H. Yang, J. Yu, Z. Li, and Z. Yu, “Non-local SAR image despeckling based on sparse representation,” *Remote Sens.*, vol. 15, no. 18, p. 4485, 2023.
- [20] M. V. Perera, W. G. C. Bandara, J. M. J. Valanarasu, and V. M. Patel, “Transformer-based SAR image despeckling,” in *Proc. IEEE Int. Geosci. Remote Sens. Symp. (IGARSS)*, 2022, pp. 751–754.
- [21] X. Jiang, S. Sun, Y. Wang, and M. Liu, “Towards federated learning against noisy labels via local self-regularization,” in *Proc. ACM Int. Conf. Inf. Knowl. Manag.*, 2022, pp. 862–873.
- [22] R. Xue, X. Bai, M. Yang, B. Chen, and F. Zhou, “Feature distribution transfer learning for robust few-shot ISAR space target recognition,” *IEEE Trans. Aerosp. Electron. Syst.*, vol. 60, no. 6, pp. 9129–9142, 2024.
- [23] Y. Pan, L. Zhong, J. Chen, H. Li, X. Zhang, and B. Pan, “SAR image despeckling based on denoising diffusion probabilistic model and swin transformer,” *Remote Sens.*, vol. 16, no. 17, p. 3222, 2024.
- [24] X. Wang, Y. Wu, C. Shi, Y. Yuan, and X. Zhang, “ANED-Net: Adaptive noise estimation and despeckling network for SAR image,” *IEEE J. Sel. Top. Appl. Earth Obs. Remote Sens.*, vol. 17, pp. 4036–4051, 2024.
- [25] W. Liang, Y. Wu, M. Li, Y. Cao, and X. Hu, “High-resolution SAR image classification using multi-scale deep feature fusion and covariance pooling manifold network,” *Remote Sens.*, vol. 13, no. 2, p. 328, 2021.
- [26] C. Zhao, X. Fu, J. Dong, S. Cao, and C. Zhang, “MLC-net: A robust SAR ship detector with speckle noise and multiscale targets,” *IEEE J. Sel. Top. Appl. Earth Obs. Remote Sens.*, vol. 17, pp. 19 260–19 273, 2024.
- [27] H. Ma, J. Qiu, S. Huang, J. Guo, and Z. Wang, “Trustfl: Robustness-enhanced privacy-preserving federated learning based on blockchain,” *IEEE Trans. Emerg. Topics Comput. Intell.*, pp. 1–16, 2025.
- [28] Z. Jia, H. Zheng, R. Wang, and W. Zhou, “FedDAD: Solving the islanding problem of SAR image aircraft detection data,” *Remote Sens.*, vol. 15, no. 14, p. 3620, 2023.
- [29] E. Bagdasaryan, A. Veit, Y. Hua, D. Estrin, and V. Shmatikov, “How to backdoor federated learning,” in *Proc. Int. Conf. Artif. Intell. Stat. (AISTATS)*, 2020, pp. 2938–2948.
- [30] S. Moreno-Álvarez, L. Han, M. E. Paoletti, and J. M. Haut, “Correlation-aware averaging for federated learning in remote sensing data classification,” in *Proc. IEEE Int. Geosci. Remote Sens. Symp. (IGARSS)*, 2024, pp. 8708–8711.
- [31] X. Gong, Y. Chen, H. Huang, Y. Liao, S. Wang, and Q. Wang, “Coordinated backdoor attacks against federated learning with model-dependent triggers,” *IEEE Netw.*, vol. 36, no. 1, pp. 84–90, 2022.
- [32] P. Blanchard, E. M. El Mhamdi, R. Guerraoui, and J. Stainer, “Machine learning with adversaries: Byzantine-tolerant gradient descent,” *Adv. Neural Inf. Process. Syst.*, vol. 30, 2017.
- [33] Y. Zeng, W. Park, Z. M. Mao, and R. Jia, “Rethinking the backdoor attacks’ triggers: A frequency perspective,” in *Proc. IEEE/CVF Int. Conf. Comput. Vis. (ICCV)*, 2021, pp. 16 473–16 481.
- [34] B. Peng, B. Peng, J. Zhou, J. Xia, and L. Liu, “Speckle-variant attack: Toward transferable adversarial attack to SAR target recognition,” *IEEE Geosci. Remote Sens. Lett.*, vol. 19, pp. 1–5, 2022.
- [35] C. Xie, K. Huang, P.-Y. Chen, and B. Li, “DBA: Distributed backdoor attacks against federated learning,” in *Int. Conf. Learn. Represent.*, 2020.
- [36] D. Davis and D. Drusvyatskiy, “Stochastic model-based minimization of weakly convex functions,” *SIAM J. Optim.*, vol. 29, no. 1, pp. 207–239, 2019.

- [37] H. Karimi, J. Nutini, and M. Schmidt, "Linear convergence of gradient and proximal-gradient methods under the polyak–lojasiewicz condition," in *Proc. Eur. Conf. Mach. Learn. Knowl. Discov. Databases*, 2016, pp. 795–811.
- [38] E. R. Keydel, S. W. Lee, and J. T. Moore, "MSTAR extended operating conditions: A tutorial," in *Proc. SPIE, Algorithms for Synthetic Aperture Radar Imagery III*, vol. 2757, 1996, pp. 228–242.
- [39] J. Zhao, Z. Zhang, W. Yao, M. Datcu, H. Xiong, and W. Yu, "Open-sarurban: A sentinel-1 sar image dataset for urban interpretation," *IEEE J. Sel. Top. Appl. Earth Obs. Remote Sens.*, vol. 13, pp. 187–203, 2020.
- [40] W. Chen, X. Xu, X. Wang, Z. Li, and Y. Chen, "Fsb: Invisible backdoor attacks via frequency domain and singular value decomposition," *Expert Syst. Appl.*, vol. 288, p. 127830, 2025.
- [41] S. Huang, Y. Li, C. Chen, Y. Gao, and X. Hu, "Fedid: Enhancing federated learning security through dynamic identification," *IEEE Trans. Pattern Anal. Mach. Intell.*, vol. 47, no. 10, pp. 8907–8922, 2025.
- [42] W. Lin, S. Wang, W. Wu, D. Li, and A. Y. Zomaya, "Hybridad: A hybrid model-driven anomaly detection approach for multivariate time series," *IEEE Trans. Emerg. Topics Comput. Intell.*, vol. 8, no. 1, pp. 866–878, 2024.
- [43] D. Yin, Y. Chen, R. Kannan, and P. Bartlett, "Byzantine-robust distributed learning: Towards optimal statistical rates," in *Proc. Int. Conf. Mach. Learn. (ICML)*, 2018, pp. 5650–5659.
- [44] T. Huang, S. Hu, K.-H. Chow, F. Ilhan, S. Tekin, and L. Liu, "Lockdown: Backdoor defense for federated learning with isolated subspace training," in *Proc. Adv. Neural Inf. Process. Syst. (NeurIPS)*, A. Oh, T. Naumann, A. Globerson, K. Saenko, M. Hardt, and S. Levine, Eds., vol. 36. Curran Associates, Inc., 2023, pp. 10 876–10 896.
- [45] Y. Meng, P. Qi, S. Zheng, Z. Cai, X. Zhou, and T. Jiang, "Adversarial attack and reliable defense based on frequency domain feature enhancement for automatic modulation classification," *IEEE Transactions on Information Forensics and Security*, vol. 20, pp. 3731–3744, 2025.
- [46] Z. Lin, J. Zheng, J. Guo, H. Lin, Y. Huang, and X. Ding, "Random response-based sar purification defense," *IEEE Geosci. Remote Sens. Lett.*, vol. 22, pp. 1–5, 2025.
- [47] F. Zeng, Y. Chen, Y. Cong, L. Zhang, S. Li, J. Xu, and J. Duan, "Stealthy backdoor attack in sar target recognition with ascm-based physically realizable triggers," *IEEE Trans. Radar Syst.*, vol. 3, pp. 947–962, 2025.



Yuchao Hou (Member, IEEE) received the Ph.D. degree from the School of Information and Communication Engineering, North University of China, Taiyuan, Shanxi, China, in 2022. He is currently an Associate Professor and M.S. Supervisor at the Shanxi Key Laboratory of Cryptography and Data Security, Shanxi Normal University. He is also affiliated with the School of Computer Science and Technology, Guizhou University. His research interests include SAR image target recognition and federated learning.



Zixuan Zhang obtained a Bachelor of Science degree from the Department of Computer and Information Engineering at Anyang Normal University, China, in 2022. Currently, she is pursuing a master's degree at the Shanxi Provincial Key Laboratory of Cryptography and Data Security at Shanxi Normal University. Her research interests include federated learning and SAR image target recognition.



Jie Wang received the Ph.D. degree from the School of Computer Science, Beijing University of Technology, Beijing, China, in 2015. She is currently a Full Professor and an M.S. Supervisor with the Department of Mathematics and Computer Science, Shanxi Normal University, Taiyuan, Shanxi, China. Her research interests include artificial intelligence and pattern recognition.



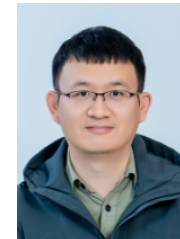
Wenke Huang is currently a Postdoctoral Researcher with Nanyang Technological University, Singapore. His research interests include federated learning and multimodal large language models. His research interests include federated learning, trustworthy and robust learning, multimodal large language models. His work has been published in leading journals and conferences, including IEEE TPAMI, IEEE TIFS, ICML, NeurIPS, and CVPR.



Lianhui Liang (Member, IEEE) received the M.S. and Ph.D. degrees from the College of Electronics and Information Engineering, Hunan University, Changsha, China, in 2019 and 2024, respectively. From 2022 to 2024, he was a visiting Ph.D. student with the Hyperspectral Computing Laboratory, University of Extremadura, Extremadura, Spain, supported by the China Scholarship Council. He is currently an Assistant Professor with the School of Electrical Engineering, Guangxi University, Nanning, China. His research interests include remote sensing image processing, signal processing, pattern recognition, and machine learning.



Di Wu (Senior Member, IEEE) received the Ph.D. degree in computer science from the University of Technology Sydney, Sydney, NSW, Australia, in 2020. He is currently with the School of Computing, Engineering and Mathematical Sciences, La Trobe University, Australia. He has authored or coauthored papers in high-quality refereed books, conferences, and journals, including top-tier venues, such as ICLR, KDD, IJCAI, WWW, and IEEE TKDE. His research focuses on federated learning, AI security and privacy, and trustworthy AI. Dr. Wu is currently an Associate Editor in NLPJ and a Reviewer for many high-quality academic conferences and journals, such as NeurIPS, ICLR, ICCV, KDD, MM, CoRL, IEEE TMC, IEEE TNNLS, IEEE TETCI, and PR.



Zhiqian Liu (Senior Member, IEEE) received the B.S. and Ph.D. degrees from Xidian University, Xi'an, China, in 2012 and 2017, respectively. He is currently a Full Professor and Deputy Dean with the College of Cyber Security, Jinan University, Guangzhou, China. His research interests include security, trust, and intelligent technologies in vehicular and UAV networks. He serves as an Area Editor or Associate Editor for several IEEE and SCI-indexed journals.



Youliang Tian (Senior Member, IEEE) received the Ph.D. degree in cryptography from Xidian University, Xi'an, Shaanxi, China, in 2012. He is currently a Full Professor and a Ph.D. Supervisor with the School of Computer Science and Technology, Guizhou University, Guiyang, China. He has authored more than 100 publications and two books. His current research interests include federated learning and privacy protection.



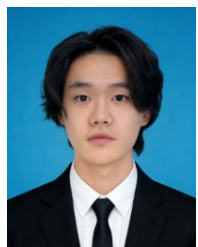
Jianming Zhu received the Ph.D. degree in computer application technology from Xidian University, Xi'an, China, in 2004. From September 2008 to March 2009, he was a Research Fellow with The University of Texas at Dallas, Richardson, TX, USA. He is currently a Professor with the School of Information, Central University of Finance and Economics, Beijing, China. His research interests include wireless network security, data privacy, and blockchain.



Jisheng Dang is with the School of Information Science and Engineering, Lanzhou University, China. He has published several papers as the first author in major journals and conferences, including IEEE Transactions on Image Processing, IEEE Transactions on Intelligent Transportation Systems, ICASSP, and ACCV. His research interests include computer vision, deep learning, and video object segmentation.



Junhao Dong received the M.S. degree in computer science and technology from Sun Yat-sen University, Guangzhou, China, in 2023. He is currently pursuing the Ph.D. degree with the College of Computing and Data Science, Nanyang Technological University, Singapore. His research interests include trustworthy artificial intelligence, computer vision, and adversarial machine learning.



Zhongliang Guo received the Ph.D. degree in computer science from the University of St Andrews, U.K. He has served as a Research Fellow with the University of St Andrews, where he worked on machine-learning-driven airspace safety and trustworthy large language models. His research interests include trustworthy artificial intelligence, adversarial machine learning, federated learning and computer vision. He has served as a reviewer for major journals and conferences, including IEEE Transactions on Information Forensics and Security, Pattern Recognition, NeurIPS, ICLR, CVPR, and AAAI, and as a Leading Guest Editor for a special issue on security and trustworthiness in Pattern Recognition.